# Chapter 11

## Coherent Radar Techniques

Erling Nielsen

Max Planck Institut für Aeronomie,
D-3411 Katlenburg-Lindau, FRG.

## Abstract

At a time when involvement of coherent radars in many research fields is expanding, it is appropriate with a tutorial review of the basic ideas and techniques in use in current coherent radar systems. After introducing the radar principles and some of the properties of radar signals backscattered from the ionosphere, data aquisition, coherent detection, digital sampling and data precessing are presented. Next the functions of various important elements in a modern radar station are described, and the fundamentals of antenna design with some much used array types are outlined. The capability of coherent radar systems for providing data, that allow estimates of the spatial variations of horizontal electron drift velocities in the ionosphere, is stressed and discussed.

## 1. Introduction

In most of the plasma regions in the space around the Earth the electrons and ions are to a very good approximation moving under influence of electric and magnetic fields in a so-called ExB drift. This is for example the case in the F-region ionosphere. However, at lower altitudes around 105 km the neutral atmosphere - even though its density is orders of magnitude below that of ions and electrons - has important effects on the mobility of ions, which totally changes the characteristics of the plasma from that at higher altitudes. Because the collision frequency of the ions with the netrual air is larger than their gyro frequency, the ion motion is governed by the electric field and the neutral air.On the other hand, the electron gyro frequency is much larger than the electron collision frequency with the neutral air, and therefore the electron motion is also at these altitudes governed by the electric fields and geomagnetic field, i.e. the electrons atmosphere of the E region that energetic particles from the magnetosphere (at high latitudes) as well as the solar radiation are mainly absorbed, and this results in strong electron density gradients. Thus, in the E region the electrons and ions are moving at a relative speed at an altitude where typically strong density gradients are present. These are the properties that distinguishes the plasma in the 95 to 120 km altitude interval from any other space plasmas associated with the Earth system. The E and F regions contain plasmas of varying properties allowing a varity of fundamental plasma physical processes to occur. Furthermore, from an observational point of view a unique aspect about these space plasmas is, that they are accessible to investigation from the ground using radio waves as well as to in situ investigations using rocket born instruments.

Coherent radars have been and continue to be essential instruments in the study of iono-spheric plasma physics. More recently it has been found that coherent radar systems can also be used to determine the horizontal flows of plasma over large areas with good spatial and temporal resolution. Since horizontal plasma flows are governed by the interaction of the solar wind with the Earth's magnetic field and ionosphere, and by other geophys-ical processes in the magnetosphere and their coupling to the ionosphere, coherent radar systems are now being used to study these processes.

The first observations of coherent radar echoes from the high latitude ionosphere were probably made during the evening hours of December 16, 1938, in Tromsø in northern Scandinavia by Harang and Stoffregen [1940]. Using a pulsed radio wave experiment with a broad beam vertical antenna (a half wave dipole with reflector) they investigated the existence of a hypothetical absorbing layer predicted to be located below the E layer. Op-erating at 41 MHz at a time of strong magnetic activity they detected weak and variable echoes from an equivalent height of between 400 and 800 km. In hindsight it seems most likely that these echoes originated from magnetic field aligned electron density irregularities in the E- and/or F-layer at ranges, or distances from the antenna, of between 400 and 800 km, i.e. from fairly small elevation angles. During the following five decades electromag-netic waves have been applied extensively to study the properties of the ionosphere using ionosondes and HF, VHF and UHF radars [Fejer and Kelley, 1980]. In particular coherent radars were used to study the equatorial ionosphere [Cohen and Bowles, 1967; Balsley and Farley, 1971; Fejer et al., 1976; Carter et al., 1976; Balsley et al., 1972; Prakash et al., 1974], the high latitude ionosphere [Unwin and Baggaley, 1972; Balsley and Ecklund, 1972; Greenwald and Ecklund, 1975; Tsunoda et al., 1974; Greenwald et al., 1978; Haldoupis and Sofko, 1976; Nielsen et al., 1983a; Greenwald et al., 1985; McNamara et al., 1983], and more recently also the mid-latitude ionosphere [Ecklund et al., 1981; Keys and Andrews, 1984; Riggin et al., 1986].

A radar operating at a certain center frequency, i.e. at a certain wavelength, is sensitive to the corresponding spatial Fourier component of the ionospheric electron density fluctua-tions along the line of sight of the radar. These spatial fluctuations in the electron density are for some physical processes so long lasting in time that the signals backscattered from a series of pulses have a high coherence. Such processes are detected with a coherent radar. It is of course the physical processes in the ionosphere which cause the signals to be coher-ent, not the radar, but the basic feature of a coherent radar is such as to take advantage of this coherency . These physical processes are excitation of plasma instabilities which result in plasma waves of relative long durations, typically several milli-seconds. In contrast the incoherent radar relies on backscatter from random, temperature fluctuations of electrons in which case there is no coherency in the signals backscattered from sequential pulses. Incoherent echoes are much weaker than coherent ones, and an incohernt radar is therefore much more complex (and also much more expensive to build) than a coherent radar.

The most fundamental measurement with a coherent radar is the auto-correlation function, or nearly equivalent, the power spectrum of the backscattered radar signals. In order to limit the amount of data output, some radars only measure the intensity of the backscat-tered signal and (essentially) the first moment of the power spectrum. These parameters can be measured as a function of distance from the radar and of azimuth (at high latitudes) or of elevation (at equator). The width of the antenna beam(s) is typically a few degrees.

Coherent radars have been operated in the interval from 8 to 1210 MHz. The range of peak power used is from 6 to 50 kW. A typical range resolution is 7.5 km, and time resolution varies from a fraction of a second to one and a half minute.

This report is intended to give a general overview and a basic introduction to coherent radar systems to those who consider using such radar systems. In the following sections the basic principles of a pulsed coherent radar and of a continuous wave radar are described, and some observations of ionospheric irregularities are presented. Next the principles of coherent detection, digital measurements and data acuisition are discussed. An example of a new coherent radar system and of different antenna designs are then outlined, and last the principles behind coherent radar measurements of electron drift velocities are discussed.

## 2. Radar Principles

Coherent radars are operated as pulsed radars or as continuous wave (CW) radars. The name 'coherent' means that the phase of the transmitted signal is preserved in a reference signal with which the received signal is compared. This reference signal is the distinguishing feature of a coherent radar. The principles in these kinds of radars are illustrated in Figure 1.

### 2.1 Pulse operations

Pulsed radars have been operated with single -, or double - pulses.

### 2.1.1 Single pulse

Let a pulse of electromagnetic waves of constant peak amplitude and of a duration $\tau$ leave the transmitter antenna at time zero, so that time is measured, for example, from the leading edge of the pulse. Ideally the flanks of the pulse should be as steep as possible to make it well defined in time, and therefore its spatial length well defined. However, since many radars are used in populated areas, and therefore should avoid to cause interference, the steepness of the flanks are reduced in order to reduce the bandwidth of the transmitted signal. The rise time at the flank is typically several micro-seconds. A pulse of width $\tau$ (measured between the 3 dB points on the flanks) covers a range $\tau$ [s] $\cdot$ c [km/s] wide in the direction of wave propagation (where c is the speed of light). If the signal is scattered from space near a distance $R_a$ from the radar, a fraction of the signal reaching that distance will propagate back towards the radar where it arrives at time $t_1 = \frac{2 R_a}{c}$. Because the backscattered signal from the trailing edge of the pulse, which also arrive at the receiver at time $t_1$, will have traveled a distance $(R_a - \Delta R) = \frac{(t_1 - \tau) c}{2}$, the spatial resolution, range gate or range cell is $\Delta R = \frac{\tau c}{2}$.

As the pulse propagates away from the transmitter antenna through a scattering medium, power is continuously backscattered towards the radar, and the final width of the pulse allows a spatial resolution of $\Delta R$, which is obtained when the signal is detected at time intervals equal to the pulse width, $\tau$. This is a typical way of obtaining the variations of backscattered signal power as a function of time, and thus of range. In order to obtain good accuracy of the power it is necessary to average the detected signal over many pulses (forming an ensemble average). It is clear, however, that if several on each other following pulses causes backscatter power to arrive at the radar at the same time, the backscatter
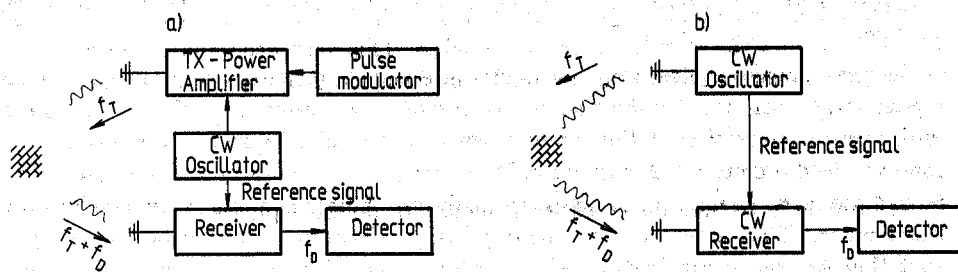
**Figure 1:** Simple coherent pulse radar (a) and CW radar (b), with emphazis on the feature that makes these radars coherent, the reference signal.

must have occurred at different ranges, and the detected power can therefore no longer be assigned to a certain range. In order to ensure the unambiguious range allocation of a signal detected at a given time, the separation in time between the pulses, the interpulse period, $T_{ip}$, must be larger than $T_{ip} \geq \frac{2\ (R_{max}-R_{min})}{c}$, where $R_{max}$ ($R_{min}$) is the maximum(minimum) distance from which backscatter can occur. The inverse of $T_{ip}$ is the pulse repetition frequency, $F_{prf} \leq \frac{c}{2(R_{max} - R_{min})}$ . While $R_{max}$ is dependent only on the extend of the medium through which the pulse propagates, $R_{min}$ is also limited by the pulse width and by how fast the receiver can be activated owing to interference from the transmitted signal (for example owing to ground reflections).

Single pulse operations are also used to obtain power spectra of the backscattered signal as a function of range. Transmitting a series of pulses with equal time spacing, yields for each range gate a time series of backscattered power, the Fourier transform of which is the power spectrum. Since the time it takes to obtain a sufficient long time series for analysis (say 128 ms), is longer than the maximum correlation time of the backscattered signal, this procedure presupposes that the physical process causing the backscatter is constant in time.

If the peak power required for a particular observation program can not be achieved with a practical transmitter for short pulses, then modulated longer pulses can be used together with pulse compression at the receiver, where the received signal is processed in a filter matched to the modulated long pulse. Pulse compression allows a radar to use long pulses to radiate large energy, while simultaneously retaining the good range resolution of the short pulse. This is achieved by use of phase modulation of the radio frequency signal, such that sub-pulses are formed within the long pulse with varying phase of the signal; the phase could for example vary between 0° and 180°. Let a long pulse be subdivided into N sub-pulses of width $\tau$, then the pulse compression ratio is said to be N, and the output of the matched filter will be a spike of width $\tau$ with an amplitude N times larger than that of the long pulse. The pulse compression ratio is typically $\gg 1$.

### 2.1.2 Double pulse

Transmitting two pulses with a time distance, $T_p$, which is an integer times the pulse width ($N\tau$) and (usually) much shorter than the Tip, additional information about the properties of backscattering medium is obtained: the velocity component of the backscattering irregularities along the line of sight of the radar. Assume that backscatter only occurs from a certain range (from a hard target); then even though $T_p < T_{ip}$ the signal received at a given time can be associated with a certain range gate. A coherent radar can in principle detect the Doppler shift in the radar frequency induced by the moving targets, and in practice the radar detects the change in phase of the returned signal from one pulse to the next. This phase change is derived from a comparison between the phase of the returned signal and the phase of the reference signal; the reference signal, in essence, determines the phase of the transmitted signal as a function of time, provided it does not suffer a Doppler shift. On the other hand a phase difference between the reference signal and the received signal then indicates that a moving target has been encountered. If for a moving hard target (for example a copper plate) the phase change is $\Delta \phi$ the velocity of the target is $V_d = $ const. $\frac{\Delta \phi}{2\pi}$. If the plate has moved a quarter wavelength during $T_p$ the distance travelled for the second pulse is a half wavelength longer than for the first, and associated

with a phase change of $\pi$ radians. In that case

$$V_d = V_a = \frac{\lambda}{4\,T_p} \tag{1}$$

Thus, for the general case

$$V_d = V_a \frac{\Delta\phi}{\pi} \tag{2}$$

Where $V_a$ is the maximum Doppler velocity, and Pi the largest phase change, one can measure unambiguously with the given values of radar wavelength and pulse separation. The smaller the pulse separation, the larger velocities can be measured.

In reality the backscattering medium is better described as 'soft' and extended in range, rather than 'hard' and limited in range as assumed above. That the target is 'soft' imply that the backscattered signal is no longer discrete in frequencies as for a 'hard' target, but has a spectral width. From the character of the spectrum (or rather the auto-correlation function) it is possible to determine a parameter, which replace the simple form of $\Delta\phi$ assumed in the previous paragraph in the calculation of $V_d$. The broad (in range) backscattering region causes the signal received at a given time to be typically composed of signals from the two pulses backscattered from different ranges. However, by cross-correlating the signal detected at times separated by $N\tau$, it is still possible to obtain the Doppler velocity as a function of range. The signal detection and data handling is outlined in Section 5.

The double pulse procedure can also be used to determine the spectrum of the backscattered signal. This is done by transmitting a series of double pulses, where the pulse separation is increasing from one pulse pair to the next, and the interval between sequential pulse pairs is larger than $T_{ip}$. One can show that each pulse pair determines one point on the auto-correlation function. The Fourier transform of the auto-correlation function is the power spectrum. The number of double pulses used has typically been 10, and for $T_{ip} = 10$ ms , it takes 100 ms to obtain one complete auto-correlation function for analysis. Since this time is longer than the maximum correlation time of the backscattered signal, this procedure also presupposes that the physical process causing the backscatter is constant in time.

### 2.1.3 Interferometer

The backscattered radar signal does not only contain information about the backscatter cross section, Doppler velocity and auto-correlation function of the backscattering medium, but also more detailed information about the direction to the backscattering region [Ierkic, 1980; Farley et al., 1981; Providakes et al., 1983; Providakes, 1985]. Assuming the backscatter originates in discreet backscatter centers, the distances travelled from such a center to two antennas, horizontally separated by typically 10s of meters, will differ by a fraction of a wavelength (plus a whole number of wavelengths). Thus, the phase difference of the signal received at the two antennas indicates the direction to the backscatter centers. If the connecting line between the antennas is perpendicular to the direction of

the antenna lobes, then the azimuthal angle from the normal to the line directed towards the backscatter irregularity can be measured. If the connecting line between the antennas is parallel to the antenna lobes, then the elevation angle to (essentially the height of) the backscatter centers can be measured.

*2.2 Continuous wave (CW)*

A CW system have been used in which the transmitter and receiver arrangements are separated by, say, 40 km along the east-west direction. East-west directed antennas are used to transmit and receive the reference signal needed for the data handling. In this configuration the system is sensitive to north-south motions of the targets. One outstanding advantage of this technique is the very high time resolution, typically 1 ms, with which one can obtain power spectra of the backscattered signal.

## 3. Ionospheric irregularities

The volumen cross-section of backscatter from the ionosphere is determined by the mean square electron density fluctuations, $< \Delta N^2 >$, and the (normalized) spatial power spectrum, f(k), of the density fluctuations [Farley et al., 1981] ,

$$
\begin{aligned}
\sigma(\underline{k}_w) &= 4\pi r_e^2 \int < \Delta N(\underline{r}) \Delta N(\underline{r} + \underline{r}') > e^{i\underline{k}\cdot\underline{r}'} \, d^3 \underline{r}' \\
&= 32\pi^4 \, r_e^2 \, < \Delta N^2 > f(\underline{k}_w)
\end{aligned}
\tag{3}
$$

where $\underline{k}_w$ is the wave vector, and $r_e$ is the classical electron radius.

From the momentum equation [Fejer and Kelley, 1980],

$$
\underline{k}_t = \underline{k}_w + \underline{k}_s
\tag{4}
$$

where t, w, and s stands for transmitted-, wave- and scattered signals. In the case of backscatter $\underline{k}_s = -\underline{k}_t$, and therefore, $k_w = 2 \, k_t$. Thus, the wavelength of the electron density fluctuations (the plasma waves) probed by the radar is equal to half the radar wavelength.

Electron density fluctuations in the E region arise owing to exitation of plasma instabilities. When the electron drift velocity, $V_e = ExB$, in the ionosphere exceeds the ion acustic velocity and/or when the scale length, $L_e$, of electron density gradients is not much larger than the signal wavelength, then plasma waves can be excited and the ionospheric plasma break up into small scale electron density structures. The wave frequency, $\omega_w$, for plasma waves propagating nearly perpendicular, i.e. within a few degrees, to the geomagnetic field, at altitudes where the ions may be considered unmagneticed, for electrons nearly free of collisions with other particles, and for wave growth rates, $\gamma$, small compared to $\omega_w$, has the form [Fejer and Kelly, 1980; Fejer et al., 1984],

$$\omega_w = \frac{\underline{k}_w \cdot (\underline{V}_e + \psi \underline{V}_i)}{1 + \psi}$$

$$\gamma = \frac{1}{1 + \psi}\left[\frac{\psi}{\nu_i}\left(\omega_r^2 - k_w^2 C_s^2\right) + \frac{\omega_r \nu_i}{k_w L_e \Omega_i}\right] - 2\alpha N_o$$

$$\psi = \psi_o\left(+\frac{\Omega_e^2}{\nu_e^2}\frac{k_{w,11}^2}{k_w^2}\right)$$

$$\psi_o = \frac{\nu_e \nu_i}{\Omega_e \Omega_i}$$

(5)

and the velocity at threshold ($\gamma = 0$) is

$$\underline{k}_w \cdot \underline{V}_d = k_w C_s (1 + \psi) F^2 + 1 + \frac{2\alpha N_o \nu_i (1 + \psi)^{1/2}}{k^2 C_s^2 \psi} - F$$

$$F = \frac{\nu_i^2}{2\Omega_i k_w^2 C_s L_e \psi}$$

(6)

where $\nu_e(\nu_i)$ and $\Omega_e(\Omega_i)$ are the electron(ion)-neutral collision frequencies and the electron(ion) gyro frequencies, respectively. $V_e(V_i)$ are the electron(ion) drift velocities, and $C_s$ the ion-acoustic velocity. The last term in the expression for the growth rate accounts for damping owing to recombination. $\alpha$ is the recombination coefficient and $N_o$ is the mean electron density. For typical values of the parameters at the altitude of the backscattering layers $\psi$ is much smaller than one.

In the absence of density gradients, $L_e = \infty$, (short wavelength approximation) the growth rate becomes positive when the wave phase velocity $\frac{\omega_w}{k_w}$ is larger than $C_s$, and so much larger as to also overcome the recombinational damping. This requirement will first be satisfied for small values of the angle $\text{Arccos}\left(\frac{\underline{k}_w \cdot \underline{V}_e}{k_w V_e}\right)$, i.e. inside a cone centered on the direction of the electron drift velocity. The approximate opening angle of the cone is $\text{Arccos}\left(\frac{C_s}{k_w V_e}\right)$. Waves propagating in this cone are called Farley-Buneman waves. If these (primary) Farley-Buneman waves are propagating across an electron density gradient, which has a component parallel to the DC electric field, then polarization electric fields, $E_p$, are formed inside the primary wave structure in directions parallel to the DC electron drift velocity. The polarization field together with the density gradients associated with the primary waves may cause the second term in the expression for the growth rate to be large enough to make $\gamma$ positive, that is to excite secondary waves. The value of $V_e$ to be used in Equation 5 is $E_p \times B$, and thus, the phase velocities of the secondary waves will be directed at large angles to the direction of the DC eletron velocity, essentially filling the angular interval outside the Farley-Buneman cone.

On the other hand, even if the DC electron drift velocity is smaller than the ion-acoustic velocity the second term of the growth rate may still cause $\gamma$ to be positive. This can occur if $k_w L_e$ is sufficient small, i.e. if Le is not too large compared to the wavelength (long wavelength approximation). In this case $\gamma$ may no longer be small compared to the wave frequency, which then has the form [Kudeki et al., 1982],

$$\omega'_w = \omega_w \frac{1}{1 + \left(\frac{k_o}{k_w}^2\right)}$$

$$k_o = \frac{\nu_i}{\Omega_i} \frac{1}{1 + \psi} \frac{1}{L_e} \tag{7}$$

This mechanism is known to operate in the equatorial ionosphere to excite long wavelength waves. Furthermore, these (primary) waves may have associated polarization electric fields (directed horizontally) large enough to excite (secondary) Farley-Bunemann waves (propagating vertically).

Waves can also be excited in plasmas at altitudes where the ions are magnetized, $\Omega_i \gg \nu_i$, [for example Fejer et al.,1984], in which case the wave frequency at marginal instability is

$$\omega_w^2 = \Omega_i^2 + k_w^2 C_s^2 \tag{8}$$

The ion cyclotron instability is generated by electrons flowing parallel to the geomagnetic field (parallel currents). The waves propagate on a cone centered on the magnetic field, and the phase velocity has a component both parallel to and perpendicular to the magnetic field. In regions, like the upper part of the auroral electrojet, where $\Omega_i = \nu_i$ the Farley-Bunemann - and the ion cyclotron instability may be simultaneously excited.

Figure 2 displays some backscatter spectra observed at high latitudes at 140 MHz. In panel a the typical spectra are shown. The thin curve is the power spectrum of the primary Farley-Bunemann waves, and the thick curve is the spectrum of the associated secondary waves. Panels b and c show unusual spectra with very small (b) and very large (c) velocities at the spectral peaks [Haldoupis and Nielsen, 1989]. Figure 3 shows some of the observed characteristics of the signal-to-noise ratio and the mean Doppler shift of the backscatter signal as a function of aspect angle, flow angle and electron drift velocity. The aspect angle is the angle between $k_w$ and the direction of the geomagnetic field. The flow angle is the angle between $k_w$ and the electron drift velocity. Panel a is in the plane perpendicular to the magnetic field and displays the variations of the mean Doppler velocity as a function of the flow angle [Reinleitner and Nielsen, 1985]. At large angles it follows a cosine law, that is the phase velocity in the direction of $k_w$ equals the component of the electron drift on that direction. At smaller angles, inside the Farley-Buneman cone, the phase velocities are limited in magnitude, at values, as shown in panel b, near the ion acoustic velocity (limited by the concentric circles). The strong dependence of the phase velocities of the primary waves on the aspect angle is demonstrated in panel c [Nielsen, 1986]. In the next two panels the strong variations of the signal-to-noise ratio for both primary and secondary waves are shown as a function of the flow angle (d) and aspect angle (e) [Andre,1983; Nielsen,1988]. The relative mean square electron density fluctuations are seen, in panel f, to increase with the electron flow velocity, and to level off, probably to saturate, at larger speeds [Nielsen et al., 1988].
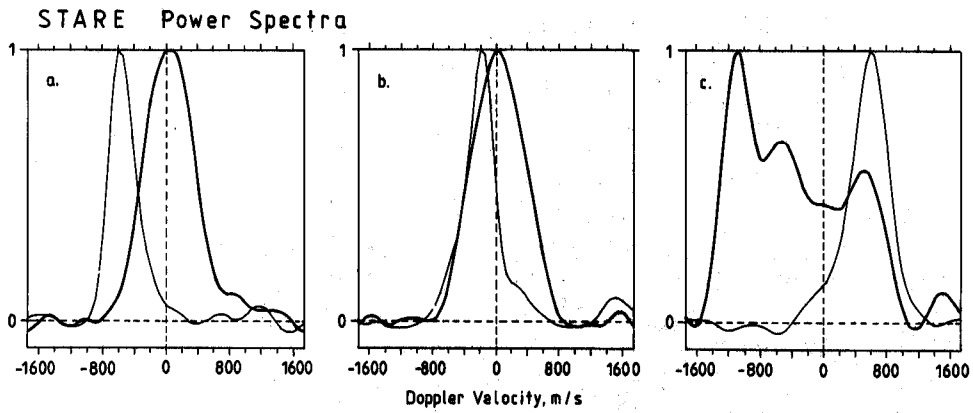
STARE    Power    Spectra



**Figure 2:** Backscatter spectra in the auroral electrojet. Panel a shows typical examples for observations at small - (thin line) and large (thick line) flow angles. In Panel b both mean Doppler velocities are small, below the ion acoustic velocity, while in Panel c the Doppler velocity in one spectral peak is much larger than any realistic ion acoustic velocity [from Haldoupis and Nielsen, 1989].
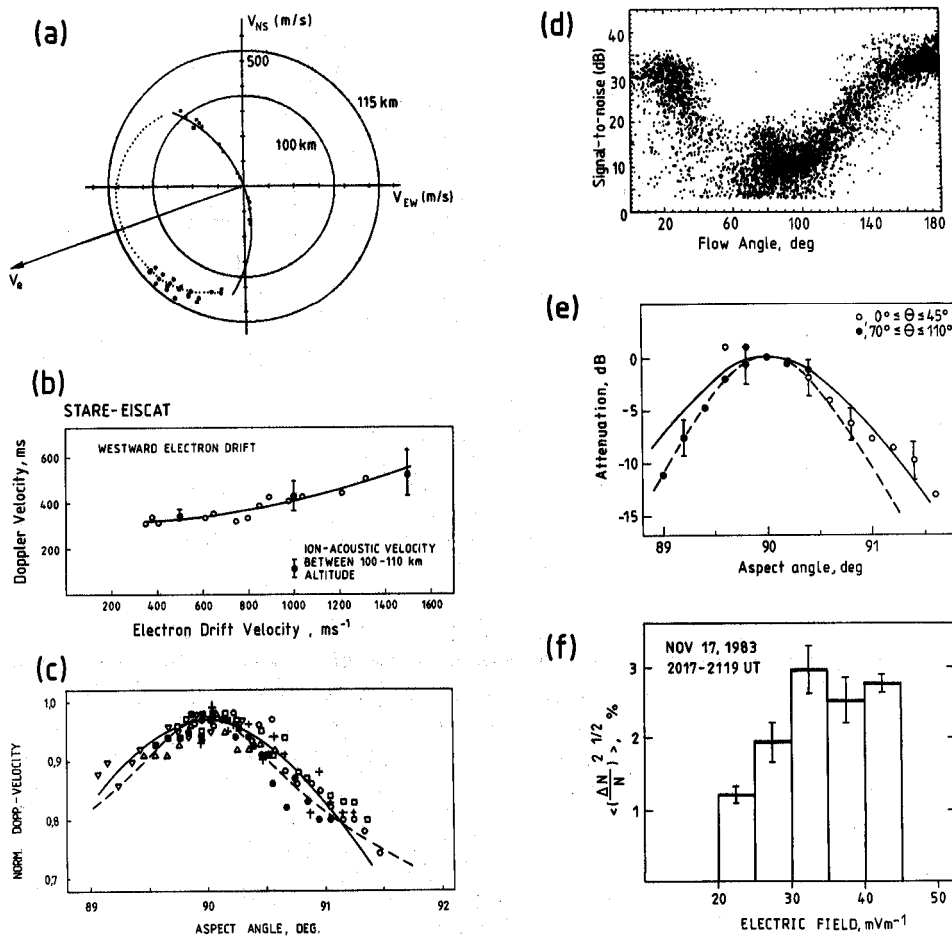
**Figure 3:** Some characteristic properties of the mean Doppler velocity and the signal-to-noise ratio as functions of electron drift speed, flow angle and aspect angle (see text).

## 4. The Radar equation

If the power of a radar transmitter is denoted $P_t$, and the gain of the transmitting antenna is $G_t$, and its radiation pattern is $g_t(\theta, \phi)$, where $\theta$ and $\phi$ are the horizontal and elevation angle, then the power density of the transmitted signal at a distance R in direction $(\theta, \phi)$ is

$$R_R = P_t \frac{G_t \ g_t(\theta, \phi)}{4\pi \ R^2} \tag{9}$$

Let the radar backscatter cross section per unit volume be $\sigma$, the backscatter volumn $V_s$, and the effective receiving area of the receiver antenna $A_e$, then the received power, $P_r$, at the antenna is

$$P_r = P_t \frac{G_t g_t(\theta, \phi)}{4\pi R^2} \frac{\sigma V_s}{4\pi \ R^2} A_e \tag{10}$$

where the effective area, $A_e$, is defined by

$$A_e = \frac{G_r \lambda^2}{4\pi} \tag{11}$$

here $G_r$ is the gain of the receiver antenna.

The antenna beam at the range of the backscatter region is normally not filled out with backscatter centers. At high latitudes $V_s$ extends across the beam in the horizontal direction while it typically may have vertical thickness, H, of 10 km. If the antenna beam width is $\Delta\theta$, then $V_s$ can be written

$$V_s = \frac{R\Delta\theta \ H_c\tau}{2} \tag{12}$$

where $\frac{c\tau}{2}$ is the depth of the backscatter volumn. The received power can now be written

$$P_r = P_t \frac{G_t \ g_t}{4\pi \ R^2} \cdot \frac{\sigma}{4\pi \ R^2} \cdot \frac{G_r g_r \lambda^2}{4\pi} \cdot \frac{R\Delta\theta \ H_c\tau}{2} \tag{13}$$

where $g_r$ is the (normalized) angular radiation pattern of the receiving antenna. The radar scattering cross section, $\sigma$, is a function of frequency or k-vector. (See also Walker et al.[1987] for a detailed treatment of the radar equation).

Moorcroft (1987) used observations from several radars operating in the range from 50 to 800 MHz to determine the relationship $\sigma(k)$ for the strongest observed signals,

$$\sigma(k) = 3 \cdot 10^{-7} \cdot k^{-2.25} [m^{-1}] \tag{14}$$

This result is shown as a solid line in Figure 4. The radar cross sections at 30 MHz were considerably larger, and at 1210 MHz lower than predicted by extrapolating from the above equation.

The figure also indicates that the possible cross section values, for a given frequency, range over 4 to 5 order of magnitudes. This spread in radar cross section results not only from its the dependence on many ionospheric parameters, but also from its depependence on the geometry between the directions of the radar line of sight, the geomagnetic field and the ionospheric electron drift velocity, as outlined in the previous section.

## 5. Data handling

### 5.1 Coherent detection

The transmitted signal of frequency $\omega$, phase $\phi$, and amplitude a(t), where the time variations refere to pulsed operations, has the form

$$s(t) = a(t)exp(\omega t + \phi(t)) \tag{15}$$

The signal arriving at the receiver antenna is a result of backscatter processes in the ionosphere and noise, can be written

$$z(t) = a_1(t)cos(\omega t) + i \ a_2(t)sin(\omega t) \tag{16}$$

This signal is amplified in the receiver and then coherently detected, as shown in the simplified schematic drawing in Figure 5.

By mixing the received signal with the reference signal, exp $(\omega t)$, phase shifted 0° and 90°, two output channels, the in-phase and the quadrature output, respectively, are formed

$$\begin{aligned} x(t) &= A(t)cos[\phi(t)] \\ y(t) &= A(t)sin[\phi(t)] \end{aligned} \tag{17}$$

where

$$\begin{aligned} A(t) &= \frac{1}{2}\sqrt{a_1^2(t) + a_2^2(t)} \\ \phi(t) &= Arctan\left(\frac{a_2(t)}{a_1(t)}\right) \end{aligned} \tag{18}$$

The bandwidths of the transmitted signal and of the receiver are both larger than the spectral width of the received signal. The results of deconvoluting the observed signal with these instrumental effects can therefore normally be disregarded.
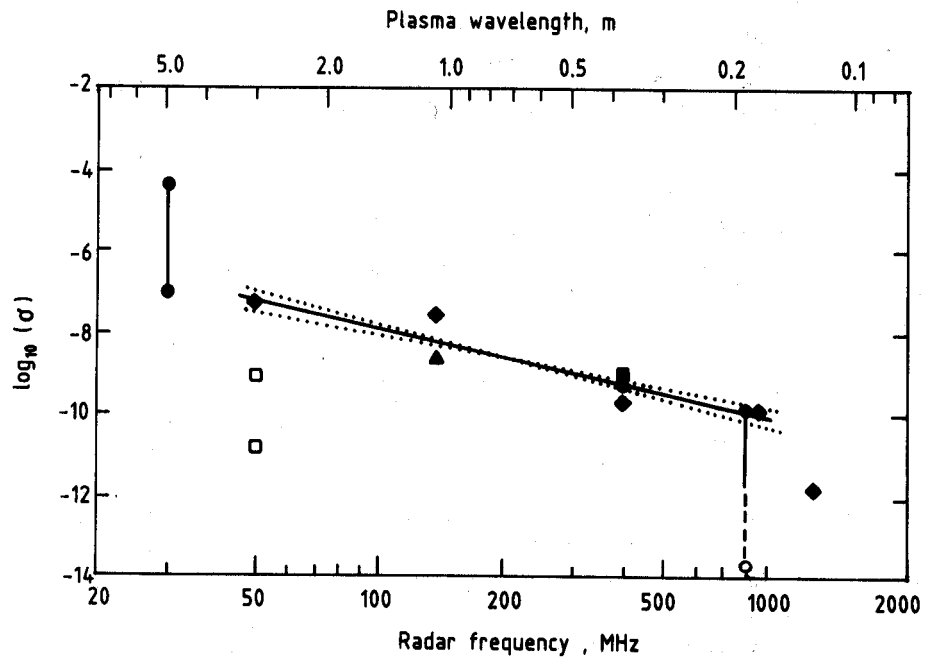
Plasma wavelength, m



**Figure 4:** Experimentally determined variations of the maximum volume backscatter cross section in the auroral region (black signature) as function of radar frequency and plasma wave length. The white signature is used for equatorial observations [from Moorcroft, 1987].
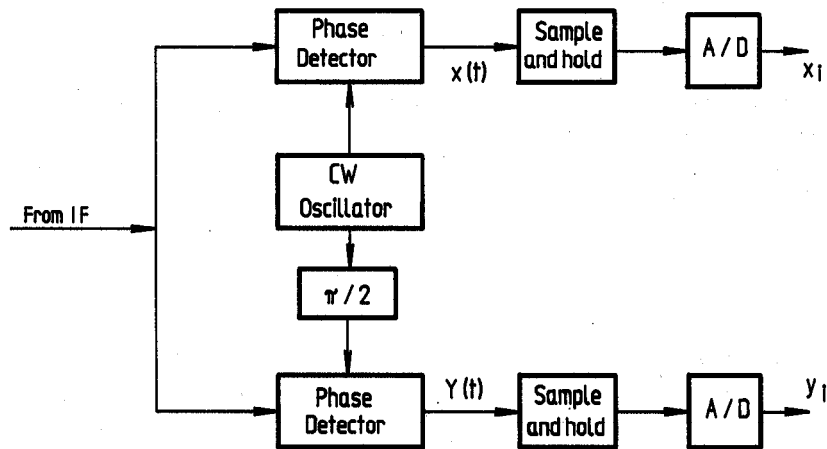


**Figure 5:** Simple block diagram of signal processing in coherent detection, producing the in-phase and the quadrature output, xi and yi, respectively.

## 5.2 Digital measurements

The time variations of the received signal is obtained by digitally sampling the input with constant time intervals equal to the pulse width. The i'th sample has the form

$$x_i = A_i cos\phi_i$$
$$y_i = A_i sin\phi_i$$

(19)

where $A_i(\phi_i)$ is the amplitude (phase) of the received signal. Conventionally the received signal and its phase are written,

$$z_i = x_i + iy_i$$
$$\phi_i = Arctan\left(\frac{y_i}{x_i}\right)$$

(20)

Independent of the transmitted pattern of pulses all information about the backscattering medium is contained in the so-called 'correlation matrix' [Turunen and Silen, 1984]. The matrix has the dimension $M \cdot M$, where $M$ is the maximum number of samples, and the matrix elements have the form $c_{ij} = z_i z_j^*$, where i=1,M and j=i,M. In the general case not all the matrix elements are of interest, many will equal zero because the signal at time 'i' and 'j' are uncorrelated. Examples of correlation matrices for single pulse, double pulse and multi(4) pulse operations are shown in Figure 6a,b and c.

## 5.3 Single pulse

For a single pulse the power as a function of time or range (of i) has the form,

$$P_i = c_{ii} = x_i^2 + y_i^2$$

(21)

In the correlation matrix the power as a function of range is located on the diagonal (Figure 6a). During one integration time (typically 20 seconds) a number of single pulses, $n_{ave}$, are transmitted; the average power from the i'th range is

$$< P_i > = \frac{1}{n_{ave}} \sum_{k=1}^{n_{ave}} (P_{ik} - Noise_k)$$

(22)

The Noise sample are measured after the pulse has passed the maximum range from which backscatter can occur.

## 5.4 Double pulse

Now, following Rummler [1968], assume that two pulses separated by an integer, N, times the pulse width are transmitted (for a pulse width of 100 micros the pulse separation may be 300 micros, i.e. N=3); the received signal at times i and j=i+N are

a) Single Pulse (Power)

b) Double Pulse (Doppler Velocity)
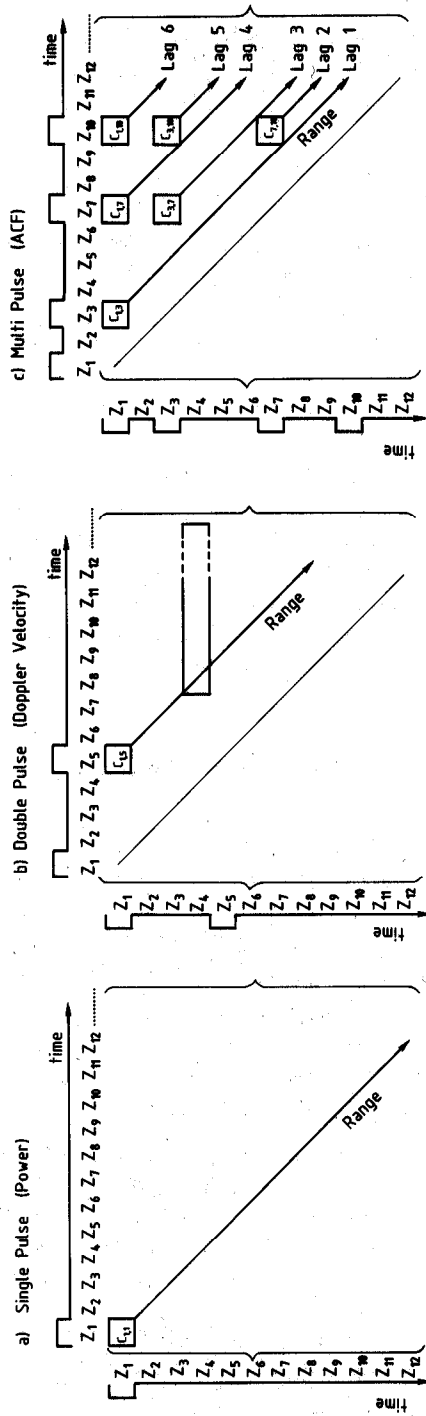
c) Multi Pulse (ACF)

**Figure 6:** The correlation matrix is illustrated for three different types of pulse patterns: single-, double-, and multi pulse. Each element in the matrix is the product of two samples taken at the same or at different times. Only those elements are different from zero for which a part of the sampled signal originated at the same range. Thus for a single pulse only $c_{i,i} \neq 0$; for a double pulse with pulse separation $4\tau$ only $c_{i,i+4} \neq 0$; for the case of a multi pulse the situation becomes more complicated as shown in Panel c. The range variation for each lag follows lines parallel to the diagonal. It is clear that only such pulse patterns are allowed for which all the 'lag-range'- lines do not overlap.

$$z_i = x_i + iy_i$$
$$z_j = x_j + iy_j \tag{23}$$

and the phase difference at these two times is

$$\phi_i - \phi_j = Arctan\left(\frac{y_i}{x_i}\right) - Arctan\left(\frac{y_j}{x_j}\right) \tag{24}$$

Now consider the multiplication of the two signals $z_i$ and $z_j^*$. One obtains,

$$c_{ij} = z_i z_j^* = (x_i + iy_i)(x_j + iy_j)$$
$$= (x_i x_j + y_i y_j) + i(x_j y_i - x_i y_j) \tag{25}$$

and noting that

$$Re(z_i z_j^*) = x_i x_j + y_i y_j$$
$$= A^2(cos\phi_i cos\phi_j + sin\phi_i sin\phi_j)$$
$$= A^2 cos(\phi_i - \phi_j)$$
$$Im(z_i z_j^*) = x_j y_i - x_i y_j$$
$$= A^2(cos\phi_j sin\phi_i - cos\phi_i sin\phi_j)$$
$$= A^2 sin(\phi_i - \phi_j) \tag{26}$$

the phase difference can be written as

$$\phi_i - \phi_j = Arctan\left(\frac{Im(z_i z_j^*)}{Re(z_i z_j^*)}\right) \tag{27}$$

and the angle of the product of the signals received at times i and j is

$$ang(z_i z_j^*) = Arctan\left(\frac{Im(z_i z_j^*)}{Re(z_i z_j^*)}\right)$$
$$= \phi_i - \phi_j = \Delta\phi \tag{28}$$

Inserting this value of the phase change in Equation 2 the target velocity results,

$$V_d = V_a \frac{ang(z_i z_j^*)}{\pi} \tag{29}$$

Since $c_{ij} = c_{i,i+N}$ these elements, or Doppler velocities, are on a line parallel to the diagonal in the correlation matrix, with the velocity corresponding to the first range located in the first row and fourth column (Figure 6b).

Now assume a broad backscatter region, i.e. that at a given time the received signal is composed of backscatter from different ranges, as illustrated in Figure 7.

The signals at time $t_i$ and $t_j$ are

$$
\begin{aligned}
z_i &= z(t_i) = S_{ia} + S_{ib} = x_{ia} + iy_{ia} + x_{ib} + iy_{ib} \\
z_j &= z(t_j) = z(t_i + T_p) = S_{jc} + S_{ja} = x_{jc} + iy_{jc} + x_{ja} + iy_{ja}
\end{aligned}
\tag{30}
$$

where indices a,b and c indicate the ranges, $R_a$, $R_b$ and $R_c$, from which backscatter originates. The product of the signal at these two times is

$$
\begin{aligned}
z_i z_j^* &= z(y_i)z^*(t_i + T_p) \\
&= S_{ia}S_{jc}^* + S_{ia}S_{ja}^* + S_{ib}S_{jc}^* + S_{ib}S_{ja}^*
\end{aligned}
\tag{31}
$$

Because the two fractions of a signal which originates at different ranges (say $R_a$ and $R_b$) are uncorrelated (because they are spatially so far apart; for $T_p = 300$ micros, 45 km), it follows that the ensemble average, the time average over the integration time, of this product is equal to the average of those terms originating at the same range, so

$$
\begin{aligned}
< z_i z_j^* > &= < z(t_i)z^*(t_i + T_p) > \\
&= < (S_{ia} S_{ja}^*) > = < (x_{ia} + iy_{ia})(x_{ja} - iy_{ja}) > \\
&= \frac{1}{n_{ave}} \sum_{k=1}^{n_{ave}} z_{ik} z_{jk}^*
\end{aligned}
\tag{32}
$$

In the time averaging of $z_i z_j^*$ it is the averages of the real and imaginary components of the product which are formed. In the general case the backscatter intensity from ranges $R_b$ and $R_c$ are as strong as from range $R_a$. Since the signal from the two former ranges are unwanted, i.e. enter the calculations as noise, 50 % of the signal measured at a given time is noise, and so the signal-to-noise ratio is no better than 3 dB.

With Equation 32 the target velocity at range $R_a$, also for a soft target, can be written as Equation 29, and since the value of the auto-correlation function of the received signal at time T has the form $R(T) = < z(t)z(t + T) >$, $V_d$ can be expressed as

$$
V_d = V_a \frac{ang[R(T_p)]}{\pi}
\tag{33}
$$

A given target velocity, v, will cause a given Doppler shift, f, of the radar frequency, which is related to the phase change, $\Delta\phi$, in the interpulse time, $\Delta t$, as

$$
2\pi f = \frac{\Delta\phi}{\Delta t} = \frac{2\pi\Delta r}{\lambda\Delta t} = \frac{4\pi v}{\lambda}
\tag{34}
$$

$$
f = \frac{2v}{\lambda}
\tag{35}
$$

At for example 140 MHz the wavelength is $\lambda = 2.14$ m, and thus f = 1.07 v.
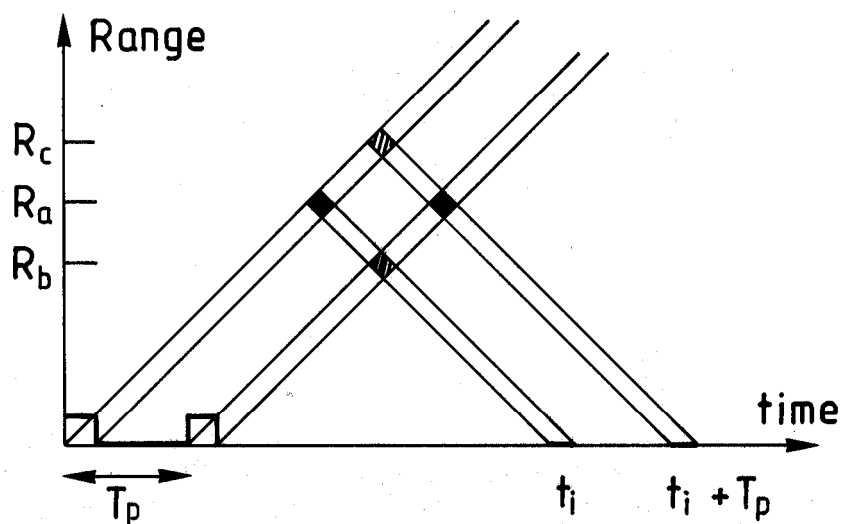
**Figure 7:** Range-Time diagram for a double pulse. It is illustrated that the signals received at $t_i$ and $t_i + T_p$ both contain backscatter signal from range $R_a$. The two signals $z_i$ and $z_i + T_p$ will therefore have a correlating part, and the time average of the product $z_i z_i^* + T_p$ will be representative of the backscatter at range $R_a$.

$V_d$ calculated according to Equation 33 is related to the mean Doppler frequency, $< f >$, of the backscattered power spectrum S(f). $< f >$ is defined by the expression

$$\int S(f)(f - < f >)df = 0 \tag{36}$$

where S(f) is normalised so that

$$\int S(f)df = 1 \tag{37}$$

The relationship between the auto-correlation and the spectrum is

$$R(T) = \int S(f)\exp(i2\pi fT)df \tag{38}$$

and introducing the definition $ang(R(T)) = 2\pi f_o T$, use $R(T)$ can be written

$$R(T) = |R(T)|\exp(i2\pi f_o T) \tag{39}$$

and therefore

$$Im[R(T) \cdot \exp -(i2\pi f_o T)] = 0 \tag{40}$$

thus, combining Equations 38 and 40 yields,

$$\int S(f)sin(2\pi T(f - f_o))df = 0 \tag{41}$$

This equation is satisfied for symmetric spectra, as well as for spectra which are only significantly larger than zero where the argument to the sine-function is small, in which case

$$\int S(f)(f - f_o)df = 0 \tag{42}$$

Comparing Equations 41 and 42 with Equation 36 indicates that $f_0 =< f >$ in these cases, i.e. the double pulse technique yields a good estimate of $< f >$ for symmetric spectra, or for any spectral shape if the requirement $T (f-f_0) \ll 1$ is satisfied. This requirement imply that the spectrum must be narrow compared to $1/T_p$ (for example: $f-f_0 \ll 1667$ Hz for T=300 micros). In practice we find, at 140 MHz, that the 'mean' Doppler velocity obtained using the double pulse technique is typically about 15 % smaller than the actual mean frequency of the power spectrum.

It was noted above that the signal-to-noise ratio for Doppler velocity measurements typically was 3 dB, independent of the gain in the radar system. The question naturally arise,

whether or not a different technique to performe these measurements could be devised such as to improve the statistics of the result for a given integration time, or to shorten the integration time and still obtain a certain accuracy. A possible way would be to mark the two pulses using different frequencies. Assuming the transmitter and antennas had bandwidths wide enough to pose no limitations, the receiver could filter the signal to separate it into components associated with the respective frequencies. These components would then be coherently detected in separate detectors, yielding for each sample two complex outputs, one associated with the first pulse only, $z_{i1}$, and one with the second pulse only, $z_{i2}$. Using $z_{i1}$ and $z_{j1}$ in calculating $V_d$ would considerably increase the signal-to-noise ratio because contributions to the signal from unwanted ranges ($R_b$ and $R_c$) would be eliminated leading to quicker convergence of the time average, allowing shorter integration times to be used.

The recognition that the time average of the received signals at time t and $t + T_p$ yields the value of the auto-correlation function for $T_p = N\tau$, the double pulse separation, it is clear that the complete auto-correlation function can be determined by using a series of double pulses with increasing pulse separation (the spectra in Figure 2 were obtained in this way). In the framework of the correlation matrix it is easy to see that the elements of auto-correlation function are located in the horizontal rectangle (in Figure 6b arbitrarily shown for the fourth range). The time required using the Stare radar system to obtain one estimate of 11 points (lags) on the auto-correlation function is, measuring for ranges up to 1230 km, about 300 ms (Nielsen et al.,1984).

## 5.4 Multi pulse

The rather detailed treatment of the douple pulse case has shown that the time average of the signals detected at time intervals equal to the pulse separation yields the important information about the signal, that is points on the auto-correlation function. In the very general case one can see that all information about the backscattering process, i.e. the auto-correlation function, as a function of range is contained in the products one can form of the time series of the digitally sampled signals. For a 4 pulse code ($n_p = 4$) one can measure the auto-correlation function at $n_l = 6$ lags ($n_l = n_p(n_p - 1)$). The correlation matrix for a 4 pulse code is illustrated in Figure 6c. The squares mark the locations of the matrix elements, which belong to the first range, and the locations of the elements with range are marked by the lines parallel to the diagonal. Farley [1972] has considered a number of multi-pulse patterns that might be used for radar auto-correlation function studies. Multi-pulses are currently being used in HF radar studies of the polar ionosphere [Greenwald et al., 1984].

It would seem concivable that the $n_e$-lag auto-correlation function could be measured faster and with the same accuracy if instead of double pulses, several pulses with interpulse separations (separations between two arbitrary pulses) from $\tau$ to $N\tau$ were transmitted together. It is also clear why this is not necessarily the case: because several pulses are transmitted the backscattered signal arriving at the radar at a given time is composed of parts from, in the general case, each of the pulses, and not only from the one pulse located at the wanted range. Thus, if for example seven pulses are transmitted into a homogeneous backscatter region the received signal has a signal-to-noise ratio of 7/6, or 0.7 db; much reduced from the double pulse case. To obtain a certain accuracy more estimates of the auto-correlation function must therefore be made in the multi pulse case

than for the double pulse case. Farley [1969] determined the consequences of this, and found the integration time to be proportional to

$$R_t = \frac{(n_p + N/S)^2}{n_p(n_p - 1)} \tag{43}$$

With the noise-to-signal ratio, $N/S = 0$, one finds for $n_p = 2$ (1 lag) $R_t = 2$, and for $n_p = 5$ (10 lags) $R_t = 1.25$. Thus, the multi pulse (5) integration time (for a given accuracy estimating the correlation) is 0.63 times the double pulse integration time. Instead of an integration time of 30 s using double pulses, for the case mentioned in the end of the previous section, one can obtained the correlation with the same accuracy in 19 s using a 5-pulse pattern.

It is speculated that the use of an 'alternating' pulse pattern [Lehtinen and Haggstrom, 1987] can even further reduce the integration time [Lehtinen, private communication].

### 5.5 Interferometer

In an altitude interferometer there are two antennas located at heights $h_1$ and $h_2$, separated by distance d and lined up in the direction of the line-of-sight. Owing to this spatial separation of the antennas the phase difference, $\Delta\phi$, between the two antennas, expressed in terms of the elevation angle, 90-$\theta$, to the backscatter centers, is [Providakes, 1985]

$$\Delta\phi_{12} = kd\cos(90 - \theta) + Arctan\left(\frac{\sin2a_1 + 2\sin a_1 \cos a_2}{1 + \cos2a_1 + 2\cos a_1 \cos a_2}\right) \tag{44}$$

where it is assumed that the ground is an ideal reflector (a good approximation at 140 MHz), and where

$$\begin{aligned} a_1 &= k(h_1 - h_2)\sin(90 - \theta) \\ a_2 &= k(h_1 + h_2)\sin(90 - \theta) \end{aligned} \tag{45}$$

For a double pulse with time separation $N\tau$ one point on the complex cross-correlation function of the signals, $z_{i,1}$ and $z^*_{i+N,2}$ (where the subscripts 1 and 2 refer to the antennas), is obtained by forming the time average of the product $z_{i,1} z^*_{i+N,2}$. Using a series of double pulses with increasing pulse separation, or a multi pulse pattern, determines the complex cross correlation function of the backscattered signal received at the antennas. The phase of the cross correlation function, i.e. the phase difference at the antennas for the i'th range , is then given by

$$\Delta\phi_{i,12} = Arctan\left(\frac{Im(z_{i,1} z^*_{i+N,2})}{R_e(z_{i,1} z^*_{i+N,2})}\right) \tag{46}$$

Equations 44 and 46 determine the zenith angle, and thus the altitude of the backscatter centers (within the uncertaincy that the phase only is measured between 0° and 360°).

## 6.   A Coherent Radar System

Stare (Scandinavian Twin Auroral Radar Experiment) is a coherent radar system consisting of two identical radar stations, which have been in operation since 1977 [Greenwald et al., 1978]. It is currently in the process of being up-graded, and has therefore been chosen here as an example of a modern radar system. The system can be used as an instrument to study plasma physics of the ionospheric E region as well as to measure electron drift velocities over a large area in the ionosphere.

### 6.1  A Radar station

Figure 8 is a block diagram of a Stare radar station. The station consists of a 50 kW transmitter which can transmit pulses 100 or 50 micros wide. These the RF signal may also be switched in phase from 0° to 180°. The signals are radiated from a broad beam antenna at low elevation angle towards the auroral zone. The backscattered signals are pre-amplified and detected in 9 independent directions, in 9 narrow antenna beams, then amplified, filtered and coherently detected in the receiver unit. The analog quadrature output from the nine channels are digitised in the correlator, a unit with the main purpose of forming the correlation matrix, that is forming the ensemble averages (Equation 32) of the (relevant) matrix elements for each channel. The output of the correlator, the auto-correlations (or maybe only the power) as a function of range for the nine channels, are written to the data storage devices, optical disks, together with a header, containing information about the time of the measurements, pulse patterns used, and the field of view, as well as housekeeping data indicating the state of the pre-amplifiers, the transmitted power and the reflected power (owing to a possible mismatch between antenna and transmitter).

The process-computer allows an operator to define the radar operations, and it then controlls these operations. At a console an operator can input the values of the physical quantities, which defines the operations (for example: near - and far range as well as the azimuthal coverage of the field of view, the pulse patterns (say a single pulse followed by multi pulse, noise measurements, and integration time). A software package translates these quantities into radar operating parameters and writes them into two files . These files, essentially, establishes the time sequence of the operations the radar has to perform, and the operations the correlator has to perform including the selection of the correlation matrix elements relevant for the chosen pulse patterns. The 'time sequence' file is copied to the memory of the radar controller and the other file to the correlator. A detailed technical description of the controller and correlator is in Schmidt et al. [1988].

The settings of the transmitter and receivers, and the time sequence of radar operations are controlled by the radar controller. It has 9 outputs going to the transmitter, receiver and the correlator. These outputs controll and/or set parameters before the start of measurements, before onset of an integration time, or during a scan (i.e. during the transmission of a group of pulses and the receiving of the backscattered signals). Before an experiment the transmitter power level is set, based on the given pulse pattern and scan time, to ensure the duty cycle of the transmitter is not exceeded, and the receiver filters are set to match the pulse width. At the end of an integration time a message is send to the correlator to start transfering the measured auto-correlation functions via the process computer to the optical disks, and the gain of the 9 receiver channels are set
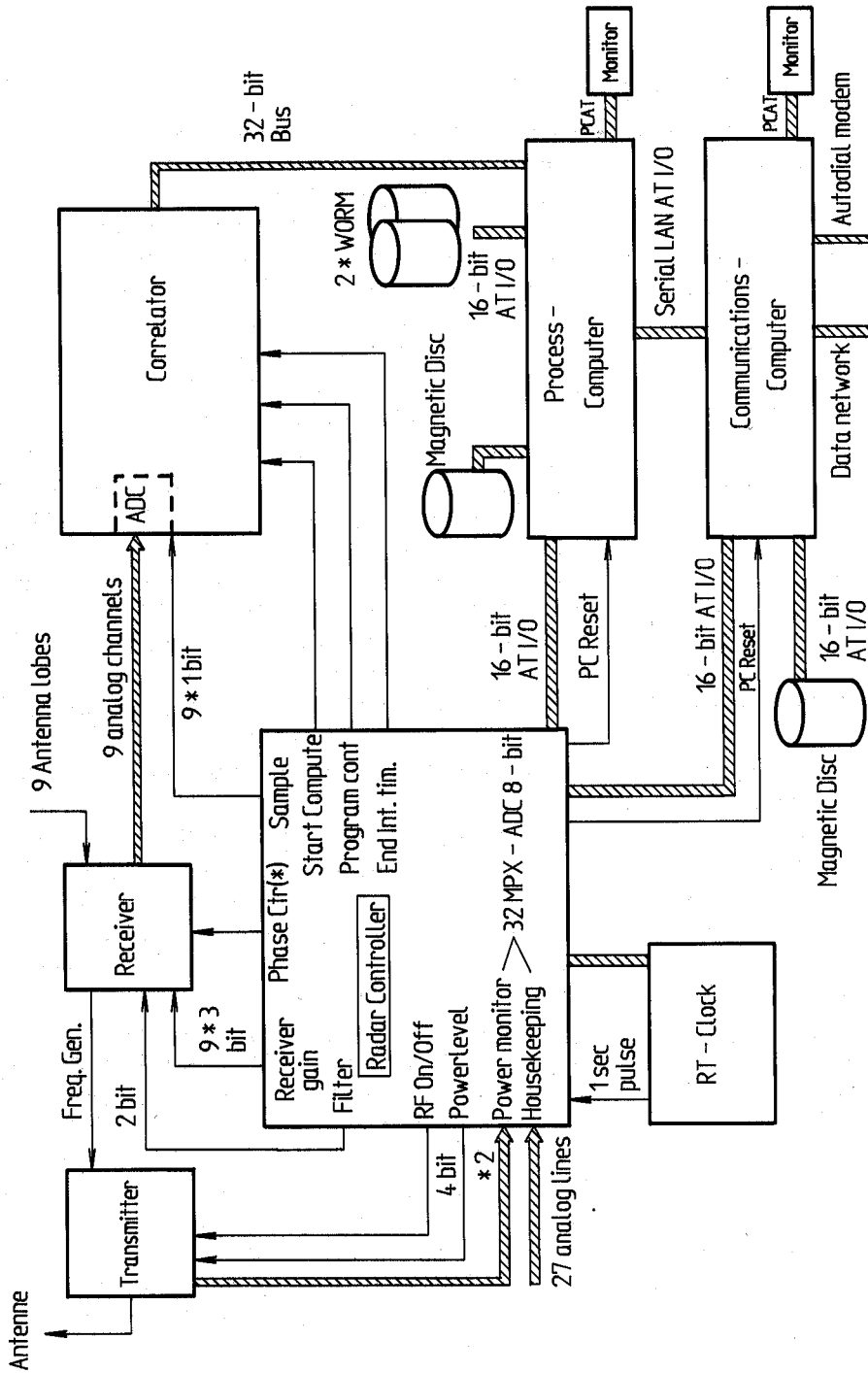
308



NEW - STARE Overview

**Figure 8:** Simple block diagram of a New Stare radar station (see text).

to optimize the receivers for the following integration time. The time sequence during one scan are determined by the content of two memories, called 'the pattern' - and 'the dwell time' memory, respectively. The operations these memories control are: the radio frequency on/off (the transmission of pulses), the phase controll of the transmitted signal, the sample times, and at the end of a scan a 'start compute' signal (or in the case an alternating code is used a 'continue' signal) is send to the correlator. Each 16 bit word in the pattern memory determines the setting of the radar controller outputs, except the power level and the end of integration time. Each bit in the word controlls one output. To each pattern-word there is a corresponding word in the (parallel) dwelltime memory, which defines the time interval during which the settings given by the pattern-word must remain at the outputs. At the end of that time interval the next words are processed, and so on untill the end of the scan. The scan is repeated a certain number of times in each integration interval.

The correlator is responsible for digitizing the coherently detected signals on the outputs of the 9 receivers, under control of the sample pulses from the radar controller. The data are stored in the data memory. The processer part carry out the complex multiplications of two complex input values, using the content of a program memory (loaded with the file generated in the process computer), which determines the addresses of the data to be multiplied. The program memory also determines the addresses in the result memory of these relevant correlation marix elements, which are then added to and stored in the result memory. The correlator is designed to handle multi pulse patterns as well as pulse compression.

The communications computer is with a local area network in contact with the process computer and its devices. This computer is used partly to display observations in real time at the radar station, and partly to facilitate remote access to the station for control of experiments or for transmission of data to an experimenter, who may for example be located at a rocket range, where real time data can be used in the decision process to launch rockets [Nielsen, 1983b].

### 6.2 Antenna

Consider a group of n similar antennas, which are oriented the same way as a reference antenna. The location of the j'th antenna is given by the vector $r_j$. The amplitude and phase of the current in the j'th antenna is given in terms of the current, I, in the reference antenna

$$I_j = \sigma_j I \tag{47}$$

Let the far field antenna pattern of the reference antenna be

$$\psi_O = I e^{i k R} \cdot F(\theta, \varphi) \tag{48}$$

where $k = \frac{2\pi}{\lambda}$, R is the distance to the point of observation, and F has its maximum value in the direction of maximum gain. Let $\varphi$ be measured in the xy-plane from the x-axis, and $\theta$ from the z-axis. The antenna field of the antenna array consisting of all n antennas is

$$\psi = \sum_{j=1}^{n} I_j e^{\frac{ik \cdot R_j}{R_j}} F(\theta, \varphi) \tag{49}$$

and using the approximation $R_j = R + r_j \cdot \hat{R}$

$$\begin{aligned} \psi &= \psi_o \sum_{j=1}^{w} \sigma_j e^{-ik r_j \cdot \hat{R}} \\ &= \psi_o g(\theta, \varphi) \end{aligned} \tag{50}$$

so the field of the array is given by the product of the field of the reference antenna and the gain function $g(\theta, \varphi)$. Let the referene antenna be at the origo of a coordinate system, where the j'th antenna has the coordinates $(x_j, y_j, z_j)$. The gain function can then be written

$$g(\theta, \varphi) = \sum_{j=1}^{w} \sigma_j e^{ik(x_j sin\theta cos\varphi + y_j sin\theta sin\varphi + z_j cos\theta)} \tag{51}$$

and the magnitude of the gain function yields the radiation pattern, a function of $\theta$ and $\phi$,

$$|g| = \sqrt{Re^2(gg*) + Im^2(gg*)} \tag{52}$$

Several coherent radars make use of an antenna arrangement producing a single narrow antenna beam, which is used both for transmitting and receiving [for example Providakes et al., 1983]. This technique has its major advantage in a good suppression of the sidelobes. In this special case all the antennas may be located on the x-axis with a constant distance, $d_x$, a constant amplitude, I/n, and a constant phase change, $\delta_x$, between all neighboring antennas, thus

$$g_x(\theta, \varphi) = \sum_{j=1}^{n} \frac{1}{n} e^{-i(j-1)(\delta_x + kd_x sin\theta cos\varphi)} \tag{53}$$

In this case it is easy to derive $\|g_x\|$, and introducing $\alpha = \delta_x + kd_x sin\theta cos\varphi$, we find that

$$|g_x(\theta, \varphi)| = \frac{sin\frac{n\alpha}{2}}{n sin\frac{\alpha}{2}} \tag{54}$$

For antennas distributed along the y- or z-axis expressions equivalent to Equation 54 for the associated gain functions can be found.

A single string of antennas will have a gain function which has essentially the form of a disk perpendicular to the direction of the string. To make the array more directional in, say, the direction of the y-axis two or more strings of antennas could be located at larger z-values and parrallel to the x-axis.

The above expressions are valid for antennas in free space. If the antennas are located over conducting ground, the mirror image of the antennas in the ground must be considered by setting (with the z-axis perpendicular to the ground) $n_z=2$, $\delta_z = \pi$, and $d_z = 2$ h, where h is the height of the antennas over the ground; the radiation pattern owing to the ground is therefore modified by

$$|g_g(\theta,\varphi)| = sin\left(\frac{2\pi h cos\theta}{\lambda}\right) \tag{55}$$

and the resulting radiation function of the string of antennas along the x-axis, also considering the radiation pattern of the reference antenna, has the form

$$|g_x'| = F(\theta,\varphi) \quad |g_x| \cdot |g_g| \tag{56}$$

The maximum gain in dB of an array with n antennas is to a reasonable approximation given by: 10 log[n]+(gain of reference antenna). The maximum gain can also be expressed by the 3 dB beamwidth's $\Delta\theta$ and $\Delta\varphi$ , measured in radians, as

$$G = \frac{4\pi}{\Delta\theta\Delta\varphi} \tag{57}$$

and the effective area, $A_e$, is

$$A_e = \frac{\lambda^2}{\Delta\theta\Delta\varphi} \tag{58}$$

To lower the sidelobe level one can use tapering, i.e. the gradual reduction of the current amplitude going from the center towards the sides of the array. This 'spatial' variation of the current amplitude could for example have the form of a triangle, of a Chebyshevs polynomium or follow a binominal law; in the latter case the sidelobes actually disappear. Tapering has in addition the unwanted effect of broadening the main antenna lobe, and therefore reducing the gain and effective area of the array.

A much used technique for constructing a string of dipole antennas, which is leightweight, portable, easy to construct and to set-up, and also fairly inexpensive, is the co-co array (coaxial-colinear array). It is constructed of coaxial cable in which the inner and outer conductor are interchanged every half wavelength, thereby producing a string of colinear halfwave dipoles. The antenna is fed at the junction between the two center dipoles. The feed arrangement consists of an impedance matching network and a balun [Balsley and Ecklund, 1972]. In such an array the current amplitude in the dipoles decreases away from the feed point owing to cable losses; thus, tapering can to some degree be controlled by choise of cable.

Antenna arrays with a single narrow beam are primarily used in coherent radars dedicated to plasma physics studies. Radar systems used to measure the spatial patterns of electron drift velocities in the high latitude ionosphere uses antenna systems with several narrow antenna lobes allowing observations to be made over a large area with good directional resolution. For example, the two Stare radar stations are located such that the lines of sight

of their antenna beams cross each other in regions of good aspect angle. Thus, backscatter from the cross-over regions can be measured from two directions simultaneously. This capability gave rise to important new possibilities for plasma physics studies, and is the property of the system that allows estimation of the electron drifts in the ionosphere.

The receiver array of the Stare system consists of 16 masts each with a stack of four yagis separated by one wavelength. The distance between neighbouring masts is one wavelength. The four yagis are combined and connected to a pre-amplifier. The output of the 16 pre-amplifiers are connected to a Butler matrix, which is a passive phasing network that forms, simultaneously, 16 narrow beams each with its separate output. Each of the narrow beams is determined by the following expression for $\alpha$ (Equation 54)

$$\alpha = (2m - 1)\frac{\pi}{16}(n_x - 1) + d_x sin\theta cos\varphi \tag{59}$$

where $d_x = \lambda$, $n_x$ varies from 1 to 16, and for beams 1 to 16 m varies from -7 to + 8. The property of the Butler matrix is such as to produce, simultaneously, the changes in phase from one mast to the next and for each beam, as given by the first term on the RHS. Inserting numerical values we find the beamwidth to be 3.2° and the separation between beams to be 3.6° (the lobes cross at the 4 dB points). The transmitter antenna is wide beam so that the transmitted signal propagates simultaneously along the receiver antenna lobes. The most important feature of the transmit/receive arrays is that, without loss of gain, one can measure in 16 independent directions simultaneously. This allows observations in two dimensions (essentially latitude and longitude) to be obtained with much better time resolution than would be possible using an electronically switched phased-array antennas. The main disadvantage is the relative poor sidelobe supression compared to that which can be obtained with phase-arrays, i.e. using the same narrow beam antenna for both transmit and receive. Note that the many lobes in the radiation pattern can also be formed by applying a software-simulation of a Butler matrix to the signals from the 16 masts [McNamare et al., 1983]. One advantage of this is the ease with which one can move all 16 antenna lobes in azimuth, and thus essentially change the field of view. The main limitation on such motions is the requirement of good aspect angle in the field of view.

At lower frequencies, in the HF frequency band (for example from 8 to 20 MHz), one is forced to use phased-arrays [Greenwald et al., 1984]. The principal reason is that a Butler matrix only can be designed for one frequency. In the HF band, however, one must be able to select the frequency which ensures good aspect angle conditions in the ionosphere, i.e. select the signal frequency which for the given electron density distribution in the ionosphere bends the signal path to make it perpendicular to the geomagnetic field lines in the region with irregularities such that backscatter occurs. Another reason is, that the strong possibility of interference from man-made noise makes it necessary to be able to select the operating frequency.

## 7. Electron drift velocities.

For the study of solar-wind/magnetosphere/ionosphere interactions it is of fundamental importance to have information on the horizontal ionospheric plasma flows. A unique

property of coherent radar systems is their ability to provide such information. The key point here is that the mean Doppler velocity of the backscattered radar signal contains information about, is a function of, the DC electric field in the backscatter region [Nielsen and Whitehead, 1983; Nielsen et al., 1983b; Nielsen and Schlegel, 1983, 1985; and Reinleitner and Nielsen, 1985]. With observations in a given backscatter volumen of the Doppler velocity from two (or more) directions, these directional velocities allow an estimate of the electric field in that volume. In the same sense, if directionally independent observations of the Doppler velocity are made in different backscatter volumens, then they can be combined to yield an estimate of the electric field if it can be argued that the field is the same in these volumes.

Figure 9 shows the horizontal radiation pattern of the Stare radars receiving arrays. The set up allows Doppler velocities to be measured from two directions in several backscatter volumes. Each pair of Doppler velocities can now be combined in one of two ways to yield an estimate of the electron drift velocity, or, since the electrons are ExB drifting, the electric field. In the first approximation Equation 5 states that the Doppler velocity in a given direction equals the component of the electron drift velocity on that direction. With two components of the electron drift the total drift velocity is determined. This estimate of the electron drift velocity turns out to yield a good estimate of the actual flow direction, but to underestimate the actual magnitude of the electron speed - the more so the larger the electron speed. However, it is important that the estimate is a lower one, it will not be some wild big number. It is a conservative estimate. The observations shown in Figure 3, panels a and b, confirm that the Doppler velocities measured at large angles to the direction of the electron flow are good approximations of the electron velocity components, but also that at smaller angles the magnitude of the Doppler velocity is primarily a measure of the electron speed (Figure 3b). With the direction of the electron flow known from the first approximation, one can now select the Doppler velocity associated with a small flow angle to determine the total flow speed, and combining this with the Doppler velocity measurement at large flow angle yields an electron drift velocity estimate, which agrees very well in direction with the actual drift velocity, and quite well (usually better than a factor two) with its magnitude.

Figure 10 shows an example of the kind of observations a VHF coherent radar system can provide. Flows in the large field of view with the good spatial resolution is measured, typically, every 20 seconds. The data allows the spatial variations in the flow to be determined at a given time, and to follow how this flow changes as a function of time. This is the unique feature of a coherent radar system.

Returning to the estimation of electron drift velocities. If only one radar station with a multi-lobe receiver array with a radiation pattern as in Figure 9 is available, an electron drift velocity can still be estimated. If the electron flow is constant along a curve (say a constant geomagnetic latitude contour) through the array lobes, and if all Doppler velocities at the given contour are measured at large flow angles in all the lobes (Equation 5 valid), then these Doppler velocities can be combined to yield an estimate of the electron flow at that contour. This is illustrated in Figure 3a, where the measurements at large flow angles are fitted in a least square procedure to a circle. The diameter of the circle (through the origo) is a measure of the electron drift velocity (as expressed in Equation 5). This technique has been widely used in single stations HF radars, and it has been shown that
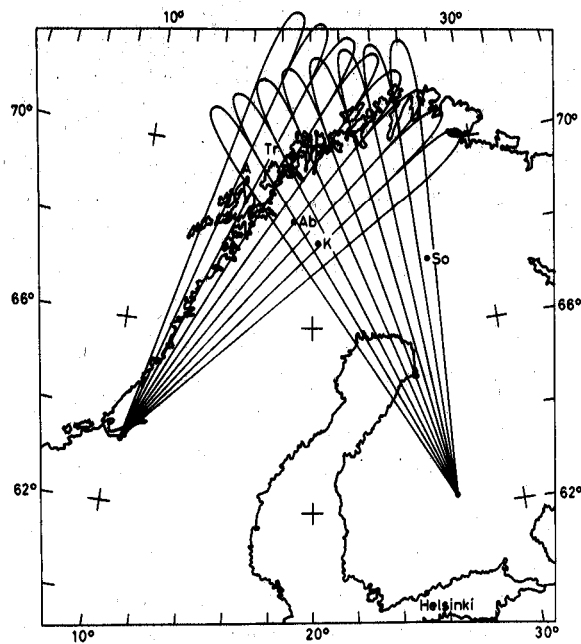
314



**Figure 9:** Map of Scandinavia showing the eight central lobes of the receiver array radiation patterns from the two Stare radar stations (from Greenwald et al. [1978])
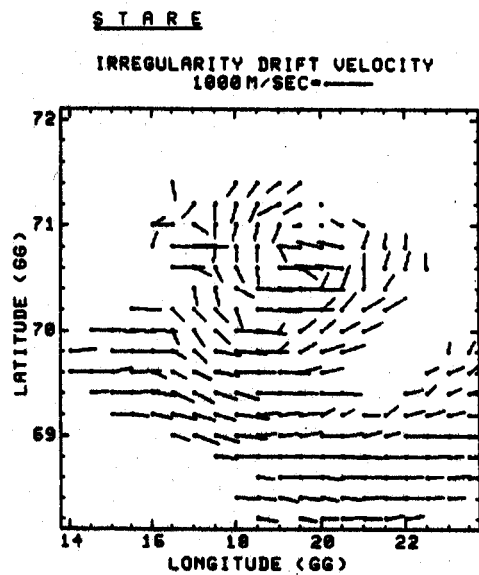


**Figure 10:** A typical example of drift velocity measurements made with the Stare radar system (from Nielsen [1982]).

even in cases where the flow on the contour is not spatially homogeneous the technique can nevertheless yield valuable information also on the spatial variations [Ruohoniemi et al., 1989].

## 8. Conclusion

Coherent radars are at present very actively used research tools. Use of these radars to study the physics of ionospheric irregularities continues. Simultaneous measurements at multiple frequencies have been made and more are planned; joint measurements with incoherent - and coherent radars will yield more detailed information about the backscattering medium than previously available, and that can also be achieved using rocket born instruments for in situ measurements. Multi-lobed array radiation patterns have so far only been used at high latitudes. They should also be employed in other parts of the Earth's ionosphere to determine the spatial variations of the radar signals and their evolution with time. The first radar system designed for electron drift velocity measurements was the Stare system, which started operations in 1977. It has been followed by similar systems, by Sabre [Nielsen et al., 1983a] and by Bars [McNamara et al., 1983]. Also at lower frequencies (HF) radars are used for geophysical studies [Greenwald et al., 1985; Dudeney, 1988]. It has been noted that a coherent radar on Kergulen Island, in the southern hemisphere, would have its field of view in the region magnetic conjugate to the Stare field of view in the northern hemisphere. With the large field of view and good spatial resolution of these radar systems detailed studies of ionospheric flows in conjugate regions could be made. Such data are at present available only from coherent HF radars with their fields of view inside the polar caps.

## 9. References

Andre, D. , The Dependence of the relative backscatter cross section of 1-m density fluctuations in the auroral electrojet on the angle between electron drift and radar wave vector, *J. Geophys. Res.*, 88, 8043, 1983.

Blasley, B.B. , and D.T. Farley, Radar studies of the equatorial electrojet at three frequencies, *J. Geophys. Res.*, 76, 8341, 1971.

Balsley, B.B. , and W.L. Ecklund, VHF power spectra of the radar aurora, *J. Geophys. Res.*, 77, 4746, 1972.

Balsley, B.B. , G. Haerendel, and R.A. Greenwald, Equatorial spread F: Recent observations and a new interpretation, *J. Geophys. Res.*, 77, 5625, 1972.

Balsley, B.B. , and W.L.Ecklund, A Portable coaxial collinear antenna, IEEE Transaction on Antennas and Propagation, 1972.

Carter, D.A. , B.B. Balsley, and W.L. Ecklund, VHF Doppler radar observations of the African equatorial electrojet, *J. Geophys. Res.*, 81, 2786, 1976.

Cohen, R. , and K.L. Bowles, Secondary irregularities in the equatorial electrojet, *J. Geophys. Res.*, **72**, 822, 1967.

Dudeney, J.R. , The Polar Anglo-American Conjugate Experiment, *EOS*, **69**, 1347, SA31A-04, 1988.

Ecklund, W.L. , D.A. Carter, and B.B. Balsley, Gradient drift irregularities in mid-latitude sporadic E, *J. Geophys. Res.*, **86**, 858, 1981.

Farley, D.T. , H.M. Ierkic, and B.G. Fejer, Radar interferometry: A new technique for studying plasma turbulence of the ionosphere, *J. Geophys. Res.*, **86**, 1467, 1981.

Farley, D.T. , Multiple-pulse incoherent scatter correlation function measurements, *Radio Sci.*, **7**, 661, 1972.

Farley, D.T. , Incoherent scatter correlation function measurements, *Radio Sci.*, **4**, 935, 1969.

Fejer, B.G. ., D.T. Farley, B.B. Balsley, and R.F. Woodman, Radar observations of two-dimensional turbulence in the equatorial electrojet, 2. *J. Geophys. Res.*, **81**, 130, 1976.

Fejer, B.G. , J. Providakes, and D.T. Farley, Theory of plasma waves in the auroral E region, *J. Geophys. Res.*, **89**, 7487, 1984.

Fejer, B.G. , and M.C. Kelley, Ionospheric irregularities, *Rev. of Geophys. and Space Phys.*, **18**, 401, 1980.

Greenwald, R.A. , and W.L. Ecklung, A new look at radar auroral motions, *J. Geophys. Res.*, **80**, 3642, 1975.

Greenwald, R.A. , W. Weiss, E. Nielsen, and N.R. Thomson, STARE: A new radar auroral nackscatter experiment in northern Scandinavia, *Radio Sci.*, **13**, 1021, 1978.

Greenwald, R.A. , K.B. Baker, R.A. Hutchins, and C. Hanuise, An HF phased-array radar for studying small-scale structure in the high-latitude ionosphere, *Radio Sci.*, **20**, 63, 1984

Haldoupis, C. , and G. Sofko, Doppler spectrum of 42 MHz CW auroral backscatter, *Can. J. Phys.*, **54**, 1571, 1976.

Haldoupis, C. , and E. Nielsen, 140 MHz auroral backscatter: Evidence for characteristic phase velocities below and above the ion acoustic speed, *Geophys. Res. Lett.*, in the press, 1989.

Harang, L. , and W. Stoffregen, Echoversuche auf Ultrakurzwellen, Hochfrequenztechnik und Elektroakustik, Akademische Verlagsgesellschaft m.b.H., Leipzig, 55, 105-108, 1940.

Ierkic, H.M. , Radar observations of the equatorial electrojet irregularities and theory of type 1 turbulence, *Ph. D. Thesis*, Cornell Uni,N.Y., 1980.

Keys, J.C. , and M.K. Andrews, Gravity wave and sporadic E echo signatures on VHF backscatter radar systems, *Planet.Space Sci.*, **32**, 1455, 1984.

Kudeki, E. , D.T. Farley, and B.G. Fejer, Long wavelength irregularities in the equatorial electrojet, *Geophys. Res. Lett.*, **9**, 684, 1982.

Lehtinen, M.S. , and I. Haggstrom, A new modulation principle for incoherent scatter measurements, *Radio Sci.*, **4**, 625, 1987

Moorcroft, D.R. , Estimates of absolute scattering coefficients of radar aurora, *J. Geophys. Res.*, **92**, 8723, 1987.

McNamara, A.G. , D.R. McDiarmid, G.J. Sofko, J.A. Koehler, P.A. Forsyth, and D.R. Moorcroft, BARS- A dual bistatic auroral radar system for the study of electric fields in the Canadian sector of the auroral zone, *Adv. Space Res.*, **2**, 145, 1983.

Nielsen, E. , M. Uspensky, A. Kustov, A. Huuskonen, and J. Kangas, On the dependence of the Farley-Buneman turbulence level on the ionospheric electric field, *J. Atmos. Terr. Phys.*, **50**, 601, 1988.

Nielsen, E. , Aspect angle dependence of backscatter intensity of 1-m auroral plasma waves, *J. Geophys. Res.*, **93**, 4119, 1988.

Nielsen, E. , Aspect angle dependence of mean Doppler velocities of 1-m auroral plasma waves, *J. Geophys. Res.*, **91**, 10173, 1986.

Nielsen, E. , and K. Schlegel, A first comparison of STARE and EISCAT electron drift velocity measurements, *J. Geophys. Res.*, **88**, 5745, 1983.

Nielsen, E. , and K. Schlegel, Coherent radar Doppler measurements and their relationship to the ionospheric electron drift velocity, *J. Geophys. Res.*, **90**, 3498, 1985.

Nielsen. E. , C.I. Haldoupis, B.G. Fejer, and H.M. Ierkic, Dependence of auroral power spectra variations upon electron drift velocity in the eastward electrojet, *J. Geophys. Res.*, **89**, 253, 1984.

Nielsen, E. , W. Guettler, E.C. Thomas, C.P. Stewart, T.B. Jones, and A. Hedberg, A new radar auroral backscatter experiment, *Nature*, **304**, 712, 1983a.

Nielsen, E. , J.D. Whitehead, L.A. Hedberg, and T.B. Jones, A Test of the cosine relationship using three-radar velocity measurements, *Radio Sci.*, **18**, 230, 1983b.

Nielsen, E. , and J.D. Whitehead, Radar auroral observations and ionospheric electric fields, *Adv. Space Res.*, **2**, 131, 1983.

Nielsen, E. , Real-time ionosphere data, *EOS*, **64**, 596, 1983.

Nielsen, E. , The Stare system and some of its applications, The IMS Source Book, AGU, 1982.

Prakash, S. , C.L. Jain, B.B. Balsley, and R.A. Greenwald, Evidence of two types of electron density irregularities in the electrojet over Thumba, India, *J. Geophys. Res.,* **79**, 4334, 1974.

Providakes, J.F. , Radar interferometer observations and theory of plasma irregularities in the auroral ionosphere, *Ph. D. Thesis,* Cornell Uni.,N.Y.,1985.

Providakes, J.F. , W.E. Swartz, D.T. Farley, B.G. Fejer, First VHF auroral radar interferometer observations, *Geophys. Res. Lett.,* **10**, 401, 1983.

Reinleitner, L.A. , and E. Nielsen, Self-consistent analysis of electron drift velocity measurements with the Stare/Sabre system, *J. Geophys. Res.,* **90**, 8477, 1985.

Riggin, D. , W.E. Swartz, J. Providakes, and D.T. Farley, Radar studies of long-wavelength waves associated with mid-latitude sporadic E layers, *J. Geophys. Res.,* **91**, 8011, 1986.

Rummler, W.D. , Two pulse spectral measurements, Tech. Memo. MM-68-4121-15, Bell Telephone Lab., Whiffany, N.J., 1968.

Ruohoniemi, J.M. , R.A. Greenwald, K.B. Baker, J.-P. Villain, C. Hanuise, and J. Kelly, *J. Geophys. Res.,* in press, 1989.

Schmidt, W. , R. Pellinen, J. Silen, and E. Nielsen, New Stare, Internal Report Finnish Meteorological Institute, 1988.

Tsunoda, R.T. , R.I. Presnell, and R.L. Leadabrand, Radar auroral echo characteristics as seen by a 398-MHz phased array radar operated at Homer, Alaska, *J. Geophys. Res.,* **79**, 4709, 1974.

Turunen, T. , and J. Silen, Modulation patterns for EISCAT incoherent scatter radar, *J. Atmos. Terr. Phys.,* **46**, 593, 1984.

Unwin, R. , and W.J. Baggaley, The radio aurora, *Ann. Geophys.,* **28**, 111, 1972.

Walker, A.D.M. , R.A. Greenwald, and K.B. Baker, Determination of the fluctuation level of ionospheric irregularities from radar backscatter measurements, *Radio Sci.,* **22**, 689, 1987.

Whitehead, J.D. , On reducing the inherent noise in the double-pulse Doppler technique, *Radio Sci.,* **18**, 93, 1983.